university of groningen

University Medical Center Groningen

University of Groningen

Structures and phase transitions in C60 and C70 fullerites

Tendeloo, G. Van; Amelinckx, S.; Muto, S.; Verheijen, M.A.; Loosdrecht, P.H.M. van; Meijer, G.

Published in:
Ultramicroscopy

DOI:
10.1016/0304-3991(93)90145-N

IMPORTANT NOTE: You are advised to consult the publisher's version (publisher's PDF) if you wish to cite from it. Please check the document version below.

Document Version
Publisher's PDF, also known as Version of record

Publication date:
1993

Link to publication in University of Groningen/UMCG research database

Citation for published version (APA):
Tendeloo, G. V., Amelinckx, S., Muto, S., Verheijen, M. A., Loosdrecht, P. H. M. V., & Meijer, G. (1993). Structures and phase transitions in C60 and C70 fullerites. *Ultramicroscopy*, *51*(1). https://doi.org/10.1016/0304-3991(93)90145-N

Copyright
Other than for strictly personal use, it is not permitted to download or to forward/distribute the text or part of it without the consent of the author(s) and/or copyright holder(s), unless the work is under an open content license (like Creative Commons).

The publication may also be distributed here under the terms of Article 25fa of the Dutch Copyright Act, indicated by the “Taverne” license. More information can be found on the University of Groningen website: https://www.rug.nl/library/open-access/self-archiving-pure/taverne-amendment.

Take-down policy
If you believe that this document breaches copyright please contact us providing details, and we will remove access to the work immediately and investigate your claim.

Downloaded from the University of Groningen/UMCG research database (Pure): http://www.rug.nl/research/portal. For technical reasons the number of authors shown on this cover page is limited to 10 maximum.

Download date: 05-05-2023

Ultramicroscopy 51 (1993) 168–188
North-Holland

ultramicroscopy

Structures and phase transitions in C_{60} and C_{70} fullerites

G. Van Tendeloo [a], S. Amelinckx [b], S. Muto [a,c], M.A. Verheijen [b], P.H.M. van Loosdrecht [b] and G. Meijer [b]

[a] *Universiteit Antwerpen (RUCA), Groenenborgerlaan 171, B-2020 Antwerpen, Belgium*
[b] *Research Institute of Materials, University of Nijmegen, 6525 ED Nijmegen, The Netherlands*
[c] *College of General Education, Osaka University, Toyonaka 560, Japan*

Received 2 September 1992

The room-temperature face-centered cubic (FCC-a_0) phase as well as the low-temperature simple cubic (SC) phase of C_{60} are studied by electron microscopy and electron diffraction. The micro-structure of the room-temperature FCC-a_0 phase is very similar to that of a low stacking fault energy FCC alloy; micro twins and stacking faults on the {111} planes are the main defects. High-resolution observations of these defects are presented here. In some parts the high-resolution images suggest a reconstructed lattice at the surface, possibly due to the presence of oxygen. The phase transition FCC-$a_0 \Rightarrow$ simple cubic (SC) at 255 K is confirmed and the observed reflections in the SC phase are only compatible with the space group $Pa\bar{3}$. A second phase transition SC $\Rightarrow$ FCC-$2a_0$ is reported. It occurs presumably at a slightly lower temperature. It is suggested that in the SC phase the molecules still have some rotational degree of freedom about their respective $\langle 111 \rangle$ rotation axis. In the FCC-$2a_0$ phase the rotation angle is assumed to be frozen in and to alternate between $+\varphi$ and $-\varphi$ along the $\langle 100 \rangle$ directions.

C_{70} can grow either hexagonally close-packed (HCP) or cubic close-packed (FCC). On cooling the HCP crystals undergo a phase transformation whereby the c/a ratio increases from 1.64 to 1.82. At lower temperatures the C_{70} molecules orient themselves inside the close-packed planes to induce a monoclinic C-centered superstructure. Above room temperature a shear transformation from ABAB... to ABCABC... occurs. Due to the ellipsoidal shape of the molecule, however, the structure is only rhombohedral with $\alpha = 88°–89°$. Only at higher temperatures does the structure gradually become FCC.

1. Introduction

The C_{60} molecule can be considered as a smooth spherical (soccer) ball with molecular point symmetry I_h. In the room-temperature phase of the C_{60} fullerite these quasi-spherical molecules are packed in a face-centered cubic arrangement [1–4]. Shortly after the discovery of the crystalline form hexagonal and even orthorhombic arrangements were reported in the literature; it is now clear that these arrangements were induced by contamination or by the presence of a significant fraction of other fullerenes, such as C_{70}. When such hexagonal material is slightly heated inside the electron microscope vacuum it transforms "in-situ" into a somewhat faulted face-centered cubic arrangement [4].

At room temperature (i.e. in the FCC phase) the molecules are assumed to rotate freely and to adopt random orientations with respect to each other; this adds to the spherical character of the molecules. On cooling below 255 K the molecules develop orientational order and the lattice becomes primitive cubic with space group $Pa\bar{3}$ [5–8].

It is the purpose of this paper to elaborate on the defect structure of the room-temperature phase of high-purity C_{60}; we will show that the defects in this material exhibit the same characteristics as in an "ordinary low-stacking-fault FCC alloy". We will further discuss defects in the simple cubic (SC) low-temperature orientationally ordered phase. Moreover, we shall demonstrate the existence of a second low-temperature phase which is face-centered cubic with a lattice parameter $2a_0$.

The C_{70} molecule is elongated like a rugby ball due to an additional ring of hexagons around the equator, when two pentagons are assumed to

0304-3991/93/$06.00 © 1993 – Elsevier Science Publishers B.V. All rights reserved

be oriented north–south. The high-temperature phase (at 440 K) is apparently FCC [9] which indicates that at this temperature the molecules are rotating along random molecular axes. At lower temperatures different phase transitions at 276 and 337 K towards lower symmetry phases have been reported [9], but there is no information on the nature of these transitions or on the crystal symmetry associated with the different phases. In this contribution we will present some room-temperature and liquid-nitrogen-temperature observations on pure C_{70}.

2. Crystal production

The C_{60} and C_{70} crystals used in this study were prepared according to descriptions given in ref. [10], whereby carbon soot is produced in a DC arc discharge between two high-purity graphite electrodes in a 0.2 atm He environment. Soxhlet extraction of this soot in boiling toluene is used to separate (mainly) C_{60} and C_{70} from the rest. This extract contains C_{60} and C_{70} in a 10:1 ratio. Liquid column chromatography [11] is used to obtain C_{60} with a purity of at least 99.5%, as checked by mass spectrometry, NMR and Raman spectroscopy. The C_{60} powder is washed with cyclohexane to remove any polyaromatic hydrocarbons that might still be present in the sample. This C_{60} material is heated in an evacuated quartz tube to 250°C for several hours to remove all the residual solvent.

During further heat treatments the quartz tube is kept at low pressure by continuous pumping. By vapour transport in the quartz tube, which is kept at one end at 500°C, pure C_{60} is formed. This process is repeated several times. The isolated very pure C_{60} is then placed in a furnace kept at 500°C for half an hour and cooled down to room temperature in about 4 h. More details on the preparation method are given in ref. [12]. Beautiful C_{60} crystals as large as $0.5 \times 0.5 \times 0.5$ mm^3 are obtained in this way (fig. 1). Samples for electron microscopy are prepared by smoothly crushing the single crystals and dipping a copper grid, covered with glue, in the powdered material. Suitable samples of C_{70} could only be obtained after crushing under liquid nitrogen; crushing at room temperature seems to affect seriously the crystalline character of the material. Microscopy experiments were performed in a Philips CM 20 analytical electron microscope and a JEOL 4000 EX or 200CX high-resolution microscope.

3. Observations on C_{60}

3.1. Room-temperature FCC phase

All X-ray and electron diffraction evidence on C_{60} high-purity single crystals at room tempera-

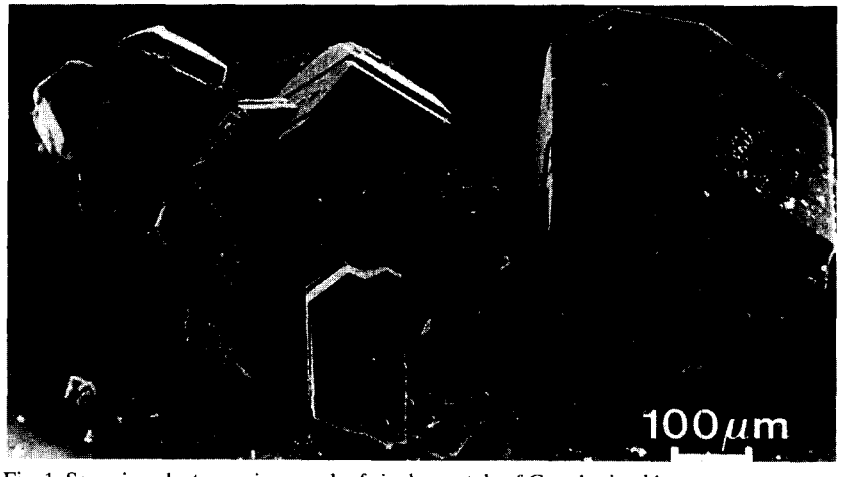

Fig. 1. Scanning electron micrograph of single crystals of C_{60} obtained by vapour transport.

ture points towards a face-centered cubic lattice with lattice parameter $a_0 = 1.41$ nm. However, a remarkable feature is observed under the appropriate conditions; the $h00$ rows of reflections are completely absent or at least extremely weak. This was noted in powder diffraction patterns by Heiney et al. [6,13]; we have confirmed this by electron diffraction. Careful tilting experiments show that although the $h00$ rows of reflections are actually present in most electron diffraction patterns, this is only because of double diffraction. Such unusual extinctions cannot be due to the presence of a particular combination of symmetry elements; it is an accidental absence. This feature results from the absence, along the $\langle 100 \rangle$ direction, of periodicity in the scattering power. Due to a particular combination of the size of the spherical molecules and of the lattice parameter, the scattering power is very nearly constant in successive $(h00)$, $(0k0)$ and $(00l)$ planes. In reciprocal space the Fourier transform of reasonable models for the spherical shell molecule has zero's at positions $h00$ for h = even. This allows one to conclude that the molecules must behave as perfectly spherical shells of diffracting power, which is consistent with the assumption that they are freely rotating about their centre, without a preference for an instantaneous rotation axis. A more detailed explanation of the structural implications of these accidental extinctions is presented in a separate paper [14]. All these considerations are only justified for kinematical scattering (e.g. X-rays); electron diffraction, however, is a highly dynamical process, particularly for larger thicknesses and multiple beam situations.

In fig. 2 we have plotted the dynamical intensity of the 200 reflection with respect to the 220 reflection in the case of electron incidence along the symmetrical [001] direction; the 200 reflection remains very weak compared to the 220 reflection. At higher accelerating voltages (400 kV) the scattering is even more dynamical than at 200 kV.

High-resolution images of such hollow C_{60} cage molecules require some caution in the detailed interpretation of "white" or "dark" dots. Image calculations for [100], [110] and [111] sections are performed to fit the experimental observations at 200 and 400 kV. 200 kV calculations for defocus

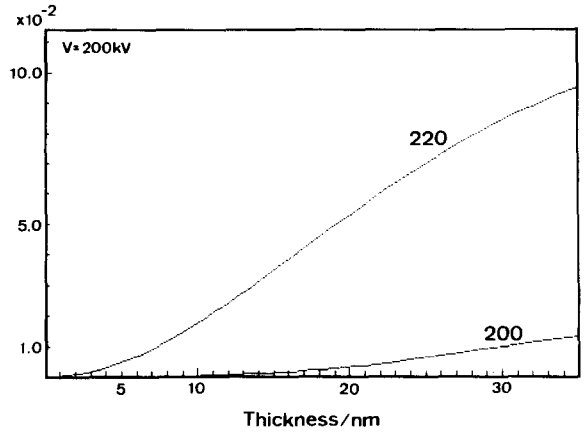

Fig. 2. Intensity plot (dynamical calculation) of the 200 and 220 reflections for [001] electron incidence at 200 kV as a function of crystal thickness.

values between -30 and -90 nm and thicknesses between 5 and 35 nm are reproduced in fig. 3. The fact that the $h00$ (and $0k0$) reflections are only present due to double diffraction has also its influence on the HREM images. Particularly for thin crystals and defocus values between -60 and -80 nm the 220 reflections mainly contribute to the image. In the experimental images these features are indeed present.

In the [111] image (fig. 3c) the bright areas correspond to channels in the structure (see ref. [4] for more details). When molecules of a different size are present also the light areas in the image aquire a different size since the channels differ. Such local regions where C_{70} columns are present in a C_{60} matrix are indicated by arrows in fig. 4. Note that this image is the only one in this paper which is taken from an impure material which was a mixture of C_{60} and about 10% C_{70}.

The most informative zone, however, is [110] (fig. 3b) since it reveals directly the stacking of the most densely packed rows of molecules. In diffraction one frequently observes streaking along one of the $\langle 111 \rangle^*$ directions. Mostly these streaks exhibit reinforcements at the positions of split FCC spots, the splitting being 1/3 of the interspot spacing along the [111]* direction. Every third [111] row remains unsplit. Such a diffraction pattern is typical for coherent (111) twinning in the FCC structure. In real space the

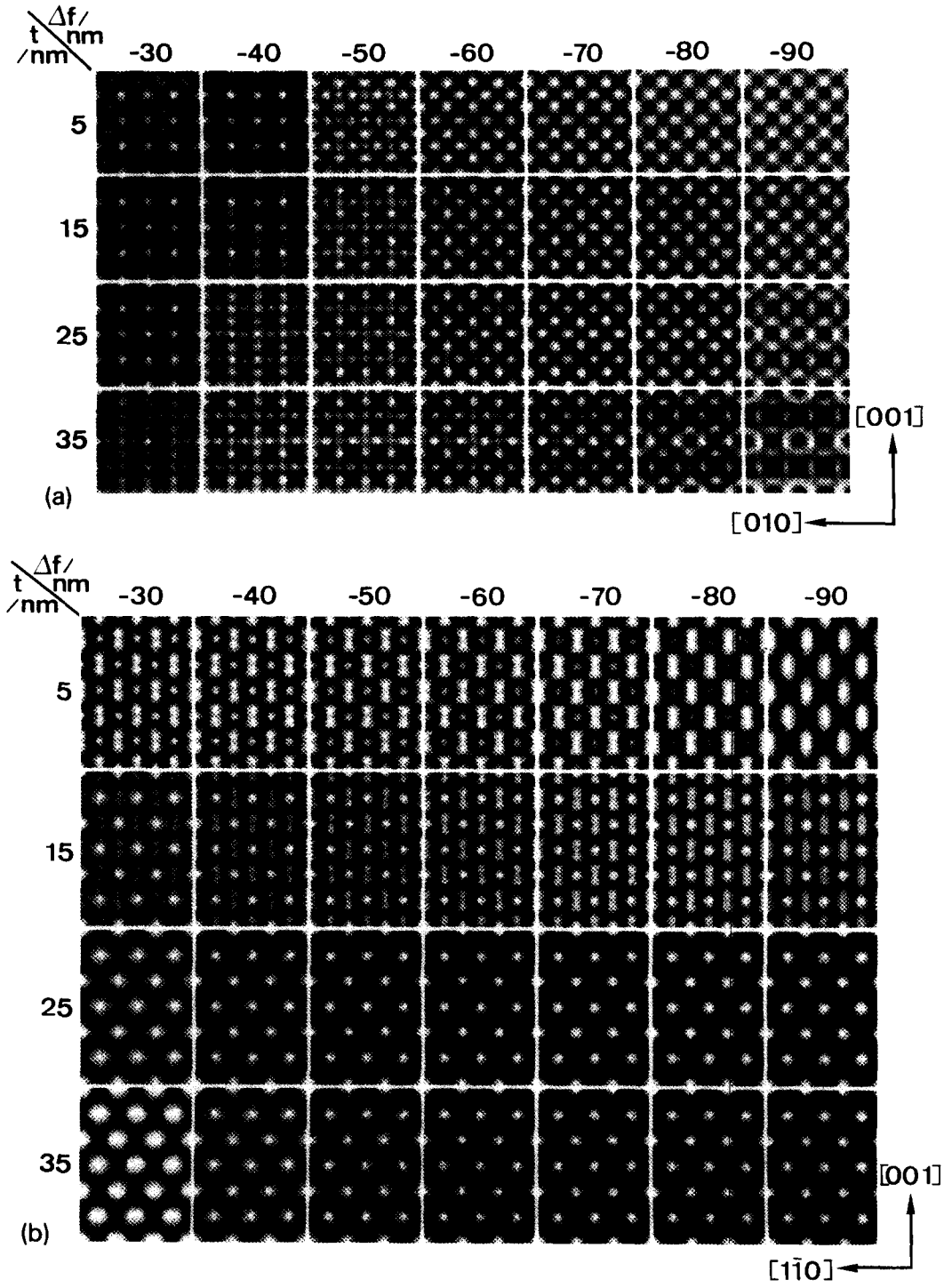

Fig. 3. Calculated images of C_{60} for (a) [100], (b) [110], (c) [111] electron incidence. Defocus values vary between −30 and −90 nm, thickness varies between 5 and 35 nm.

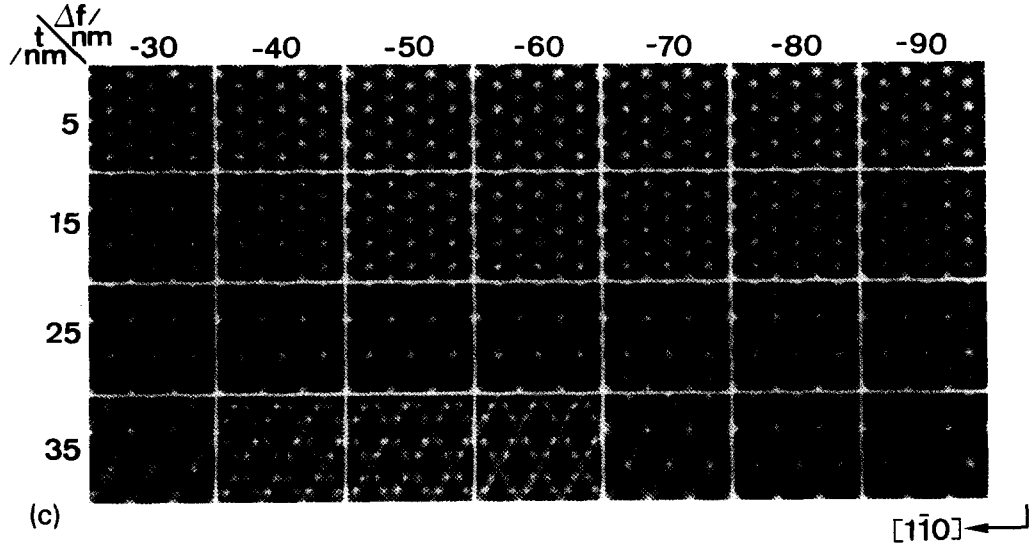

Fig. 3 (continued).

crystals are found to contain most of the types of defects which commonly occur in the face-centered cubic metals and alloys with low stacking fault energy, the most prominent feature in our samples being coherent microtwinning and stacking fault formation (fig. 5). The faults are of

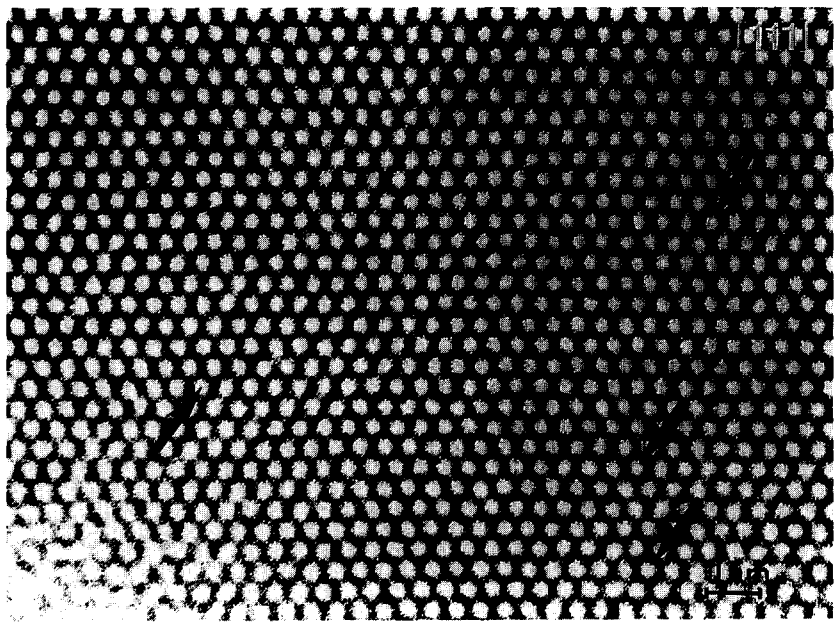

Fig. 4. High-resolution image of C_{60} crystal containing 10% of C_{70} viewed along the [111] zone. Note the local differences in dot brightness attributed to the presence of C_{70} molecules.

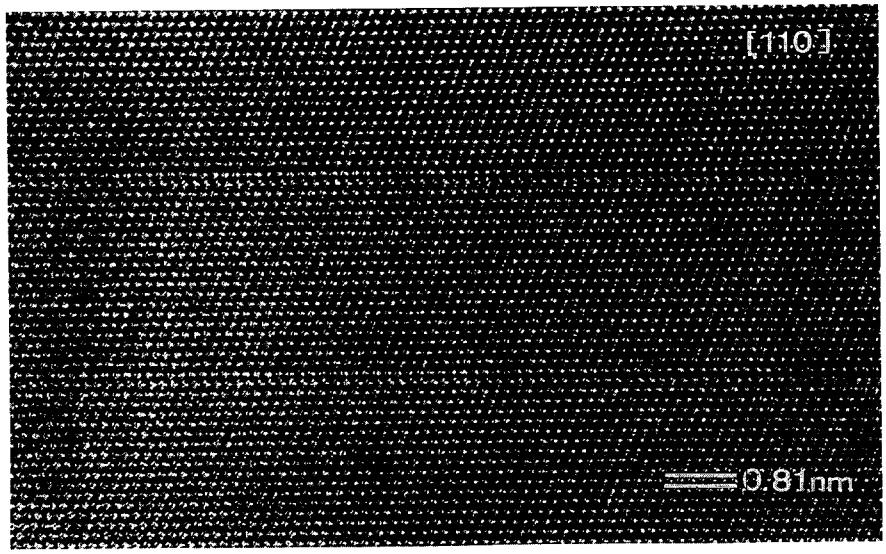

Fig. 5. Stacking faults in pure C_{60} imaged along [110].

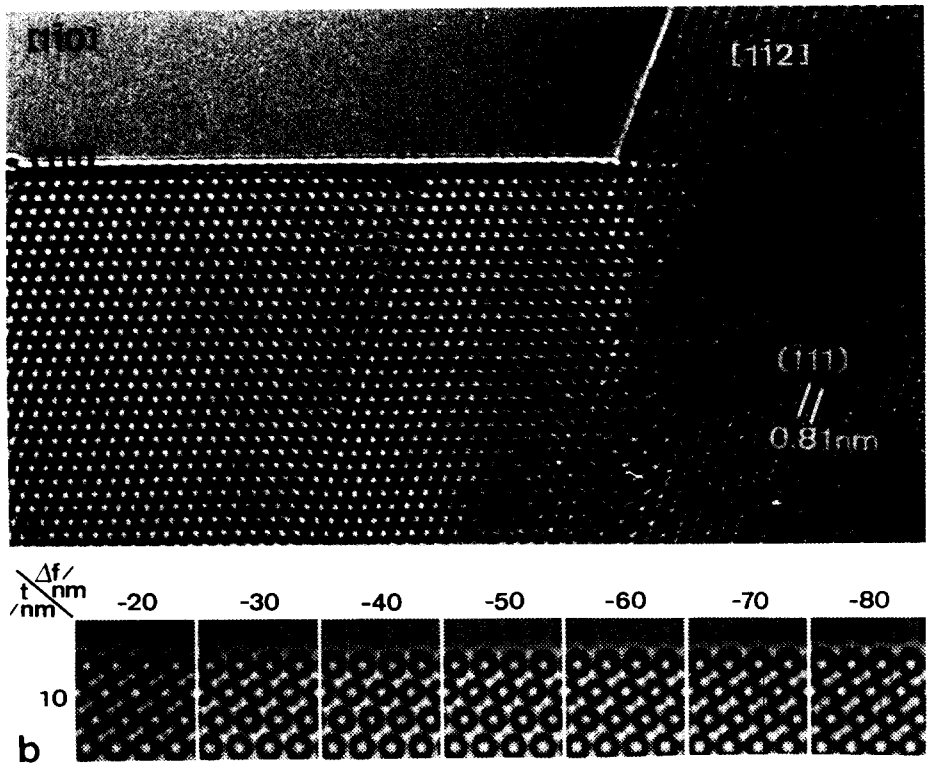

Fig. 6. (a) Reconstruction at the (111) surface of a C_{60} crystal imaged under [1$\bar{1}$0] incidence. (b) Calculated images for a thickness of 10 nm and defocus values between −20 and −80 nm.

the intrinsic type ABCABABC, which implies that they could have been formed by the propagation of Shockley partials.

The similarity between the defects in C_{60} and in FCC-based alloys with low stacking fault energy is quite remarkable even though in the former case we have to do with van der Waals bonded molecules and in the latter case with atoms in metallic bonds. Both types of bonds are non-directional, however.

A remarkable observation is shown in fig. 6a. The crystal orientation is close to [1$\bar{1}$0] and the high-resolution image can be compared to the calculated images of fig. 3, at least inside the material. At the surface, which is parallel to (111), the image contrast clearly deviates from the contrast inside. There is a heavy black–white line running parallel to the surface and the top bright dot is shifted away from its normal position. We have calculated the image for a surface layer of pure C_{60} along the [110] orientation; it is shown in fig. 6b. Clearly no unusual behaviour is to be expected if the top layer would be "just" C_{60}; also other thicknesses show no unusual effects. The present image therefore indicates a reconstruction of the C_{60} surface over the top one or two layers. Such observations are only visible when the surface is planar and parallel to a low-index plane such as (111). The origin of the reconstruction is not clear; however, it is believed that it is triggered by the presence of impurity atoms (oxygen? solvent residues? ...) at the sur-

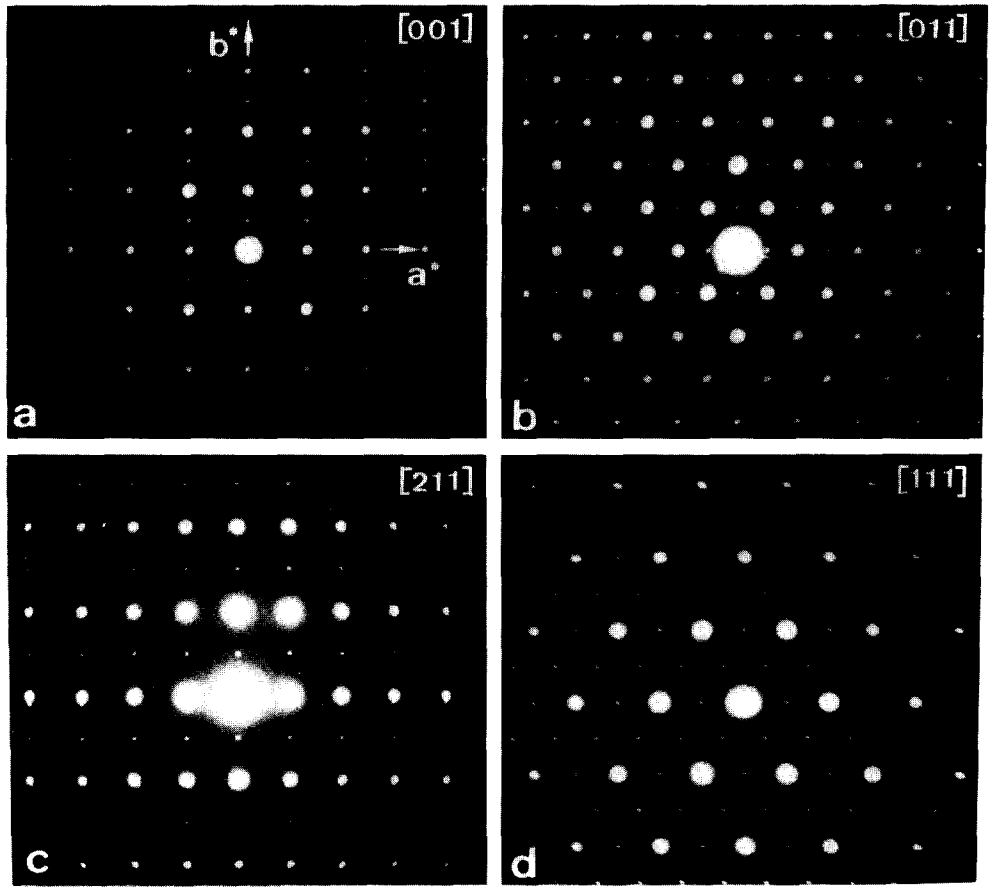

Fig. 7. Electron diffraction patterns of the simple cubic low-temperature phase. (a) [001] zone; note the presence of the $0k0$ row with k = odd due to double diffraction. All reflections with h = odd are systematically absent. (b) [011] zone. (c) [211] zone. (d) [111] zone.

face. What we image as a surface structure, however, is clearly the reconstruction of the C_{60} surface and not necessarily the direct image of possible foreign atoms, since the top surface layer has the same periodicity as the bulk C_{60}. Note on the right side of the image the presence of a particular grain boundary between two different crystal orientations with parallel $(\bar{1}11)$ planes and with $[1\bar{1}0]$ parallel to $[1\bar{1}2]$.

3.2. The low-temperature simple cubic structure

On cooling high-purity C_{60} single crystals inside the electron microscope the existence of a low-temperature primitive cubic phase with symmetry $Pa\bar{3}$ [6,8,15,16] has been confirmed unambiguously.

On cooling the sample in the electron microscope below 255 K weak additional reflections

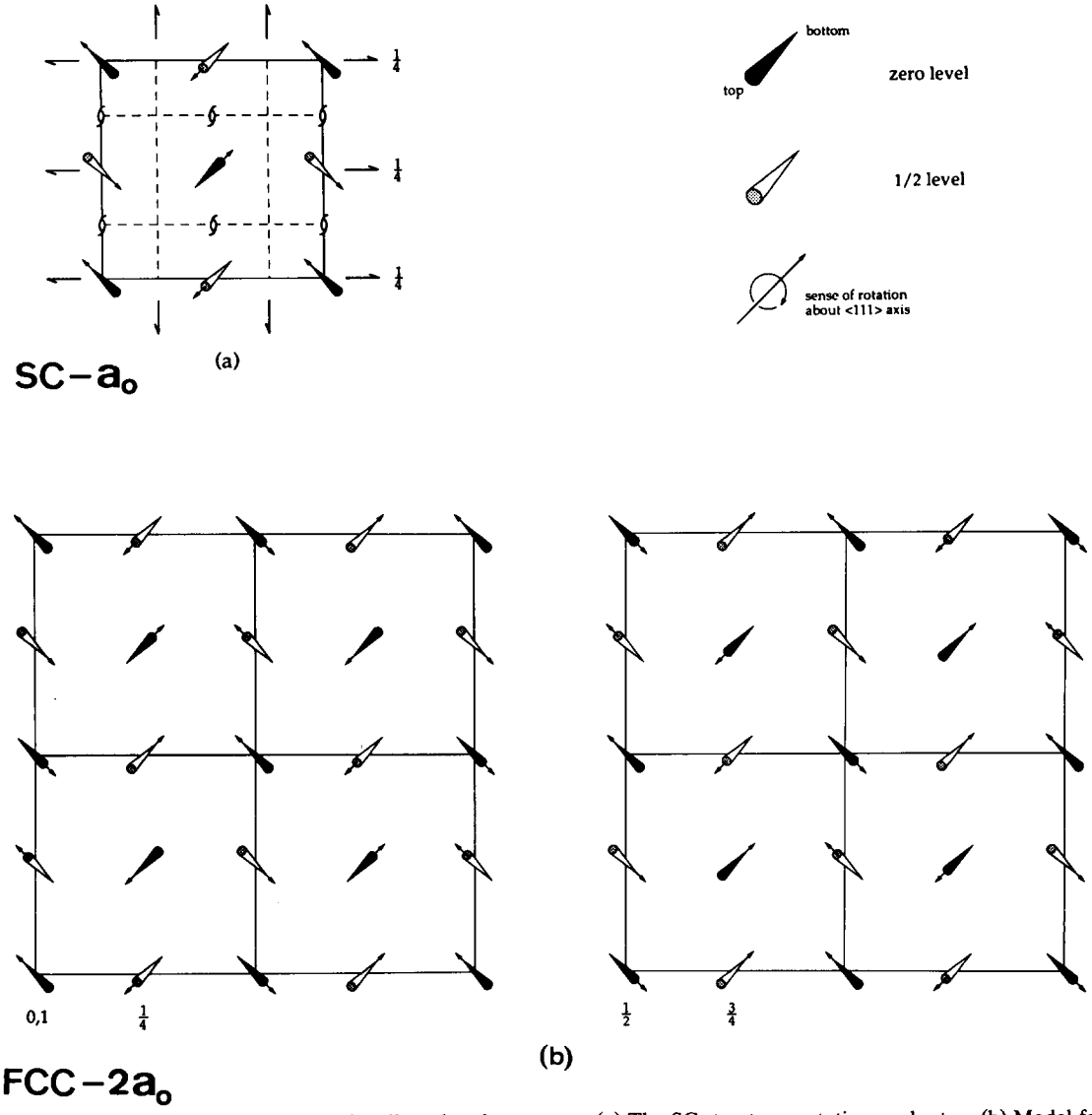

Fig. 8. Schematic representation of orientationally ordered structures. (a) The SC structure, rotation angle $+\varphi$. (b) Model for the FCC- $2a_0$ superstructure at level 0, 1/4 (left) and at level 1/2, 3/4 (right).

appear in most zones. The most relevant sections of reciprocal space are shown in the sequence of diffraction patterns of fig. 7 obtained by tilting the same crystallite. It is quite obvious that the most intense spots still form a body-centered cubic lattice, i.e. the reciprocal lattice of a face-centered lattice. However, the weaker additional reflections occupy positions which are forbidden for a face-centered structure. All spots of this type can be indexed on the basis of a primitive unit cell with (approximately) the same lattice parameters as the FCC cell. In the (001)* section (fig. 7a) $hk0$ reflections are present for h = even. The $0k0$ reflections, k = odd, are visible in most diffraction patterns, but it could be shown by tilting experiments that they are formed by double diffraction. The reflection conditions thus have to be completed with $0k0$ reflections present only for k = even. This set of diffraction conditions unambiguously identifies the space group as $Pa\bar{3}$, which confirms the suggestion made in a comment on ref. [6] by Sachidanandam and Harris [15].

In the simple cubic (SC) structure the four sites of the parent FCC lattice become non-equivalent; molecules occupying these sites will be called respectively A, B, C and D. In the simple cubic structure each of these positions is now occupied by one type of molecule. According to ref. [6] the A, B, C and D molecules differ in their orientations and the FCC–SC transition is therefore an orientational order–disorder transition.

The orientational transition can be described as follows. In the reference orientation three mutually perpendicular binary axes of the molecule are parallel to the cube directions ⟨100⟩ of the lattice. The threefold axes of the molecules are then parallel to ⟨111⟩ directions of the lattice. In this orientation all molecules are equivalent and the lattice is still FCC. The symmetry can now be broken by rotating the four different molecules A, B, C and D about four different ⟨111⟩ directions over an angle φ.

The direction of the rotation axis and the senses of the rotations of the different molecules are, of course, related by the symmetry elements of the space group $Pa\bar{3}$. In fig. 8a the upper and lower ends of the bars, which are projections of ⟨111⟩ directions, indicate the sense of the inclinations. The arrows indicate the sense of rotation over the angle φ, by the right-hand rule.

The number of rotation variants is equal to the order of the point group of the high-temperature phase, which is 48, divided by the order of the point group of the low-temperature phase, which is 24. This yields two different orientation variants. These variants are related by one of the rotational symmetry operations lost during the transformation. In the present case the simplest choice is a rotation over 90° around one of the twofold axes of the point group $m\bar{3}$, which is parallel to a cube direction. The two orientation variants can thus be termed 90° rotation twins. For each orientation variant four translation variants are possible; they are related by the FCC symmetry translations $[\frac{1}{2}\ \frac{1}{2}\ 0]$, $[\frac{1}{2}\ 0\ \frac{1}{2}]$, $[0\ \frac{1}{2}\ \frac{1}{2}]$, lost during the transformation. The total number of equally probable variants is thus 8.

In a molecular crystal such as C_{60} still another type of structural variant, related to the orientation of the molecule itself, has to be considered. For such a highly symmetrical molecule the rotation angle can with the same probability be $+\varphi$ or $-\varphi$. The two structures in which the senses of the rotation angles differ are "a priori" equally probable and satisfy the same space group. It should be noted that the molecule as well as the structure contain a centre of symmetry. The two structures are thus not enanthiomorphic and they are, for instance, not related by a mirror operation.

The standard method to reveal orientation variants is to make dark-field images in reflections specific for a single variant (e.g. 120 and 210). The domains which produce intensity in the selected spot will then show up bright. In the present case such experiments were repeatedly performed but failed to reveal well defined domain walls; the bright and dark patches observed were irregularly shaped and not bordered by sharp interfaces. The apparent absence of crystallographic interfaces is possibly related to the fact that the symmetry of the crystal lattice remains cubic on transformation. After a transformation accompanied by a symmetry decrease the sharp

interfaces are determined by the requirement that they should be strain-free; such interfaces are not defined if the lattice remains cubic, as in the present case. The absence – in general – of sharp, well defined domain interfaces is furthermore related to the ease with which the spherical molecules are reorienting.

This irregularity is no longer the case if twin boundaries or stacking faults are inherited from the basic structure. The presence of such boundaries in the basic structure apparently induces a change in the orientation pattern of the molecules which causes these boundaries to become also domain boundaries of the orientationally ordered superstructure. In fig. 9a the sample is in the orientationally ordered phase, as is apparent from the corresponding $[2\bar{1}\bar{3}]^*$-type diffraction pattern of fig. 9c. The image of (a) is formed using a 120 superstructure reflection, which is encircled in fig. 9c. It is clear that bright and dark bands are present which are limited by planar defects along (111) planes. One could at first sight interpret this banded contrast as being due to the presence of twins in the basic structure; however, imaging is performed in a superstructure reflection. Moreover, when the sample is heated above the transformation temperature of 255 K, without changing the diffraction conditions, all contrast disappears, even though the lattice defects remain (see fig. 9b). The corresponding diffraction pattern is reproduced in fig. 9d; superstructure reflections are no longer visible. This experiment

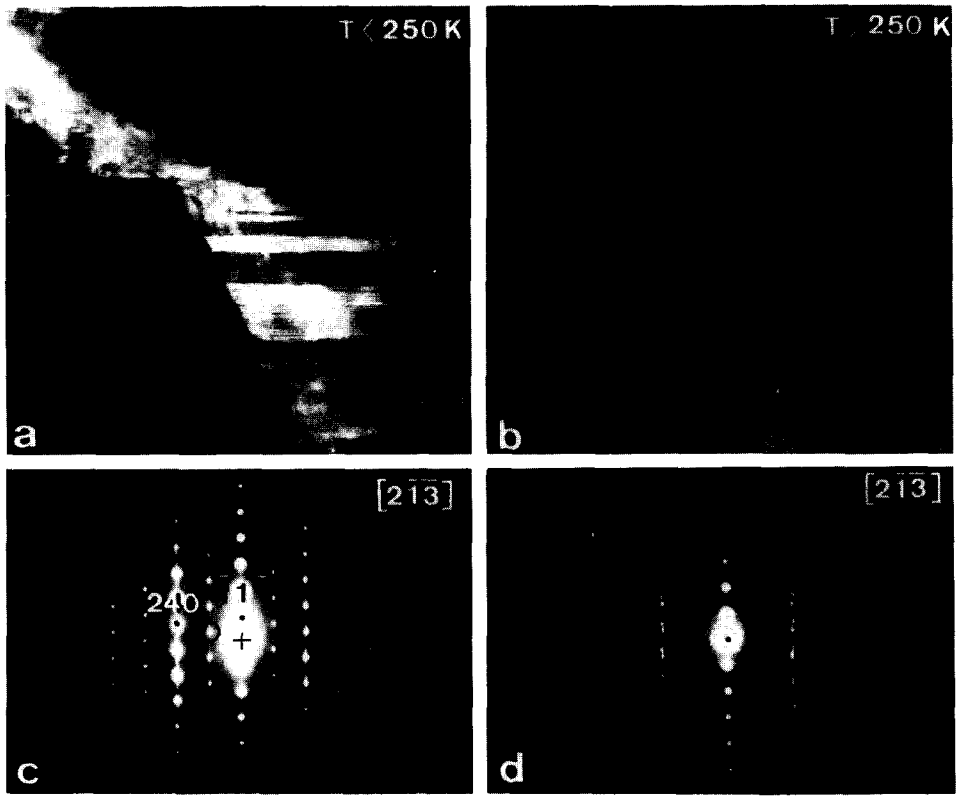

Fig. 9. Diffraction experiment showing the relation between twin interfaces in the basic structure and orientation domain walls in the SC phase. (a) Dark-field image at liquid-nitrogen temperature in a 120 reflection surrounded by a small circle in the corresponding diffraction pattern (c). (b) Dark-field image under the same diffraction conditions above the 255 K transition. In the corresponding diffraction pattern at room temperature (d) all superstructure reflections have disappeared.

is consistent with the interpretation of the bright areas as ordered domains of the selected variant.

3.3. The low-temperature $2a_0$-FCC phase

Careful examination of diffraction patterns of specimens cooled to liquid-nitrogen temperature revealed the presence of weak reflections which are not consistent with a simple cubic (SC) structure. In particular in the [110]* section of reciprocal space the rectangular meshes are centered by weak but unambiguously identifiable spots (fig. 10). These spots cannot be due to spikes from higher-level zones in reciprocal space; they are also not due to reflections introduced by twinning or faulting in the basic structure, since initially unfaulted crystals were selected. These weak extra spots become, relative to the basic and the superstructure spots, more intense with increasing length of the diffraction vector. This is a characteristic of periodic displacement-modulated structures. Such displacements can, for instance, be caused by a finite rotation of the molecule around an axis.

The relative weakness of the supplementary reflections indicates that the superstructure cannot deviate much from the simple cubic, orientationally ordered structure, which was described above. Single-crystal X-ray measurements by Liu et al. at 110 K [16] and by De Boer [17] failed to detect this superstructure. We therefore propose a model for this superstructure which involves the least changes with respect to the model for the SC structure. We retain the configuration of rotation axes but in order to double the lattice parameters – as we observe – we assume that along the ⟨100⟩ rows the molecules are alternatingly rotated over different angles, e.g. over $+\varphi$ and $-\varphi$. This model is represented schematically in fig. 8b. In this way orientationally equivalent molecules are dispersed as uniformly as possible

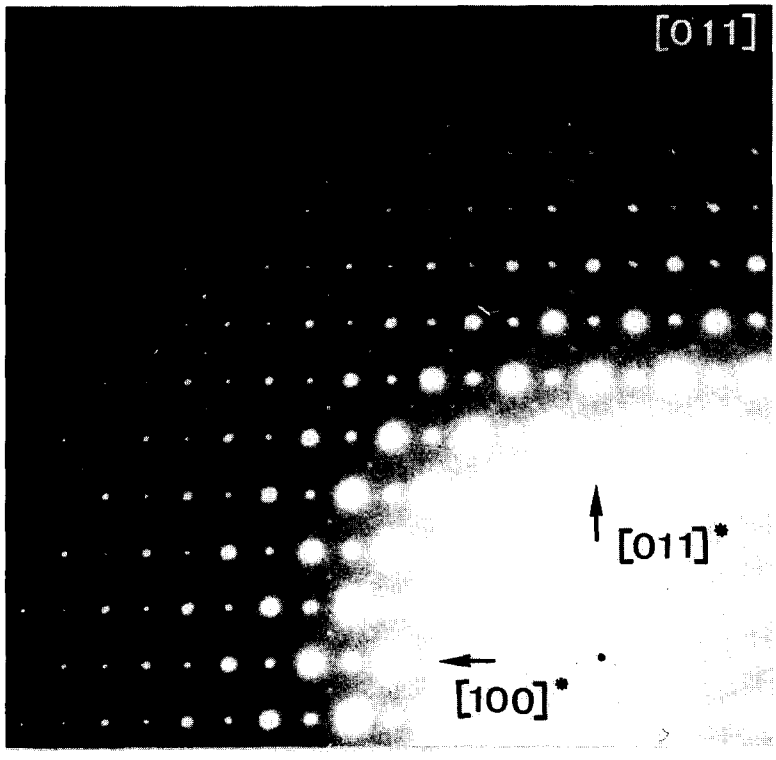

Fig. 10. Diffraction pattern along the [011] zone taken at liquid-nitrogen temperature. Note the weak superstructure spots due to the FCC-$2a_0$ phase. The SC-a_0 structure reflections have been surrounded.

throughout the structure. Molecules of a given orientation form a face-centered cubic arrangement with a lattice parameter $2a_0$. The structure consists of eight such interpenetrating face-centered cubic lattices, each occupied by a given type of oriented molecule. A single crystal of such material will presumably be fragmented in a large number of variants, translation as well as orientation variants, due to the orientation of the rotation axis and the sense of rotation of the molecules in the different sublattices. Since the diffraction patterns of the different variants produce coincident spots, this will not be apparent from the electron diffraction pattern. The fact that single-crystal X-ray diffraction does not detect the present ordering is an indication that the ordering takes place in very small domains. It is furthermore not impossible that the present superstructure and the SC structure co-exist. Imaging of the ordered domains in the microscope failed because of the weak intensities and the sensitivity of these reflections to electron irradiation.

Electron diffraction experiments down to liquid He temperatures confirmed the presence of these reflections, but did not reveal the formation of other superstructure reflections, which might be expected on the basis of theoretical predictions [18].

4. Observations on C_{70}

As mentioned above, the C_{70} molecular cage has an elongated shape [9]. Structural considerations favour packing of such molecules in close-packed layers in which the long axis of the pseudo-ellipsoids of revolution are parallel. The layers themselves are expected to be stacked according to the HCP mode, the long axis being parallel to the hexagonal c-axis. This model assumes the molecules to be either static or rotating about their length axis. If this model corresponds to reality, one expects the c/a ratio of the HCP stacking to be significantly larger than the ideal value for close-packed spheres. If, on the other hand, one assumes that at room temperature the molecules are freely and isotropically rotating, the c/a ratio would have a value close to the ideal value for close-packed spheres ($c/a = 1.63$). Also the stacking fault energy in the

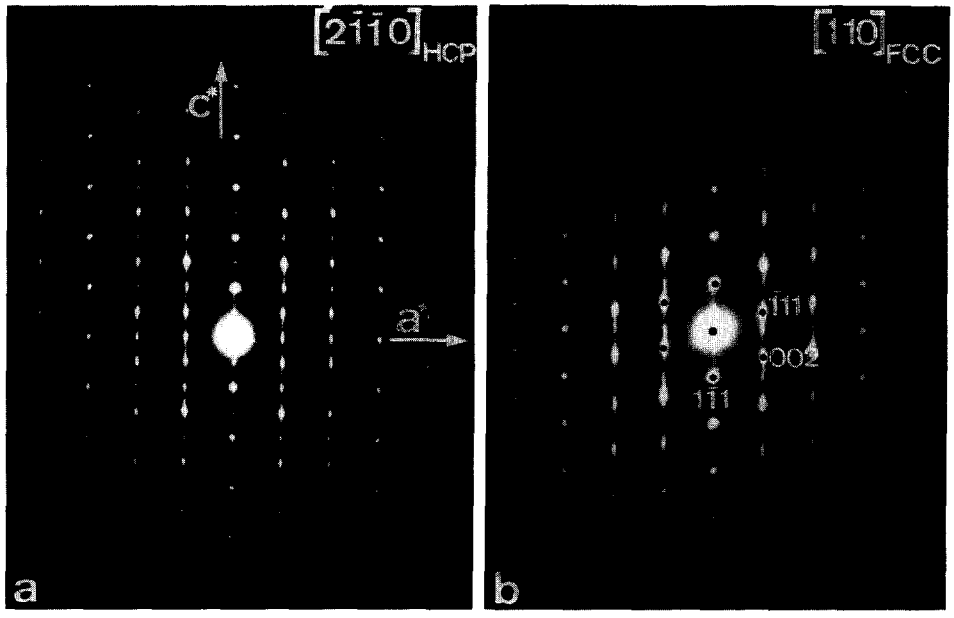

Fig. 11. (a) $[2\bar{1}\bar{1}0]_{HCP}$ diffraction pattern of C_{70} at room temperature. (b) $[1\bar{1}0]_{FCC}$ diffraction pattern from a neighbouring area.

hexagonal phase would then be very small, as is the case for stacking faults in the FCC structure of C_{60}.

4.1. Room-temperature structure

The electron diffraction patterns from a crushed single crystal depend on the selected area within the same crystal. We observe patterns such as figs. 11a and 11b.

The first pattern can be indexed on a hexagonal close-packed lattice, noting that the weak $000l$ reflections with l = odd have to be attributed to double diffraction. However, two out of three rows contain elongated reflections, streaked along c^*; in every third row spots remain round and sharp. The rows of reflections perpendicular to c^* are not quite straight; the streaked spots undergo slight displacements in opposite sense in the direction c^*. These observations show that an appreciable fraction of the crystal is faulted leading to slight peak shifts of the centres of gravity of the streaked diffraction spots parallel to c^*, towards the FCC spot positions.

The second type of pattern (fig. 11b), made along the same zone axis, is at first glance to be indexed as the [110] section of an FCC crystal. Also in this pattern streaks are present along $[1\bar{1}1]^*$ in the rows of reflections for which $h-k$ is not a three-fold. This pattern proves that the selected area is predominantly stacked in the cubic mode, but that extensive faulting (either stacking faults or microtwins) is present on the {111} planes common to the twins. Careful measurements on this and other diffraction patterns (e.g. the [001] section of fig. 12b) indicate that the symmetry is not cubic but slightly rhombohedral ($\alpha = 88°$–$89°$), the deviation from cubic symmetry being small and a function of temperature. The higher the temperature the smaller the rhombohedral distortion. This rhombohedral distortion is visible in the diffraction patterns (fig. 12b) as well as in the high-resolution images (fig. 12a).

As pointed out above, the value of the c/a ratio is quite informative concerning the geometry and shape of the stacked units. From fig. 11a we deduce c/a 1.64 ± 0.02; the corresponding ratio in the pseudo-cubic phase of fig. 11b as measured on the sharp spot arrays is 1.66 ± 0.02,

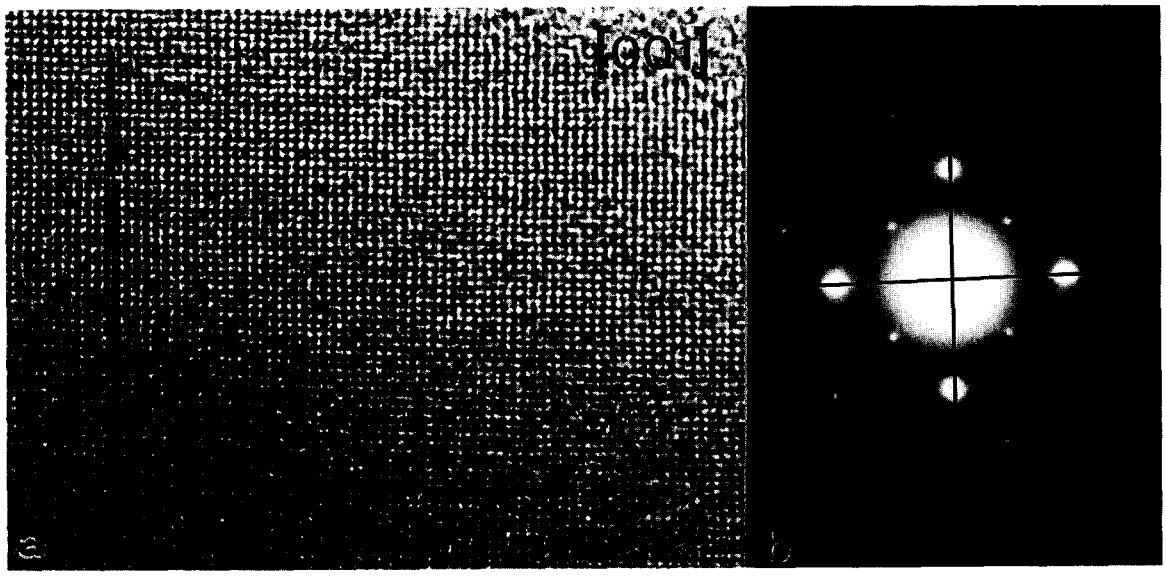

Fig. 12. (a) HREM of rhombohedral C_{70} at room temperature imaged along the $[001]_{FCC}$ direction. (b) Corresponding electron diffraction pattern.

i.e. the ratio is slightly different from that for the hexagonal stacking. Since the a-parameter (i.e. the intralayer spacing) is the same for both phases, the difference is due to a difference in interlayer spacing.

The high-resolution images along the zone parallel to the close-packed rows (i.e. to [110] in the FCC phase) are the most informative ones since they reveal the stacking mode directly. Such an image is shown in fig. 13a at low magnification whilst a higher-magnification image is reproduced in fig. 13b. The area clearly exhibits two different stacking modes (HCP and FCC) as well as a number of faults in both stacking variants. Calculated images confirm the interpretation as an HCP phase. Especially the somewhat unexpected rectangular configuration of bright dots in fig. 13b was shown to represent the HCP phase for small foil thicknesses and for defocus values around -60 nm (see ref. [20]).

The hexagonal bands contain double layer defects of the type ABABABCACAC..., i.e. defects containing two triplets in the cubic stacking mode. Such defects can be generated by glide of

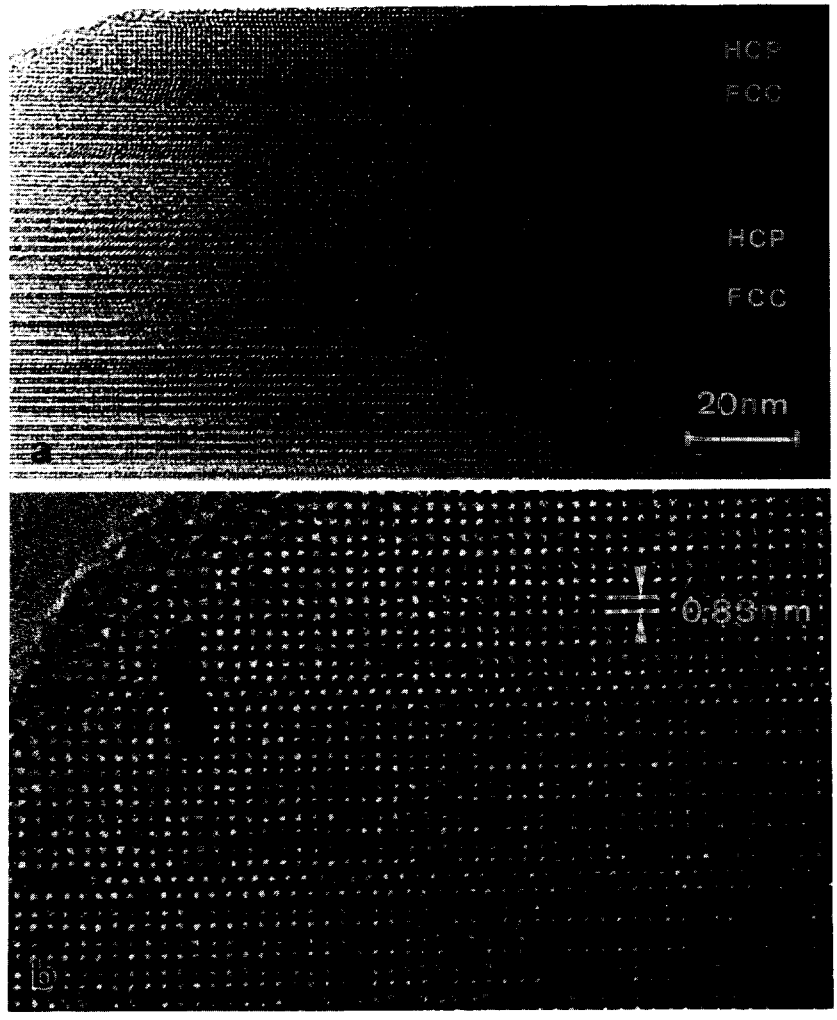

Fig. 13. (a) Low-magnification high-resolution image along $[2\bar{1}\bar{1}0]_{HCP}$ or $[110]_{FCC}$ showing the interweaving of FCC and the HCP bands. (b) High-resolution image of a HCP stacked region; two stacking faults are indicated by arrows.

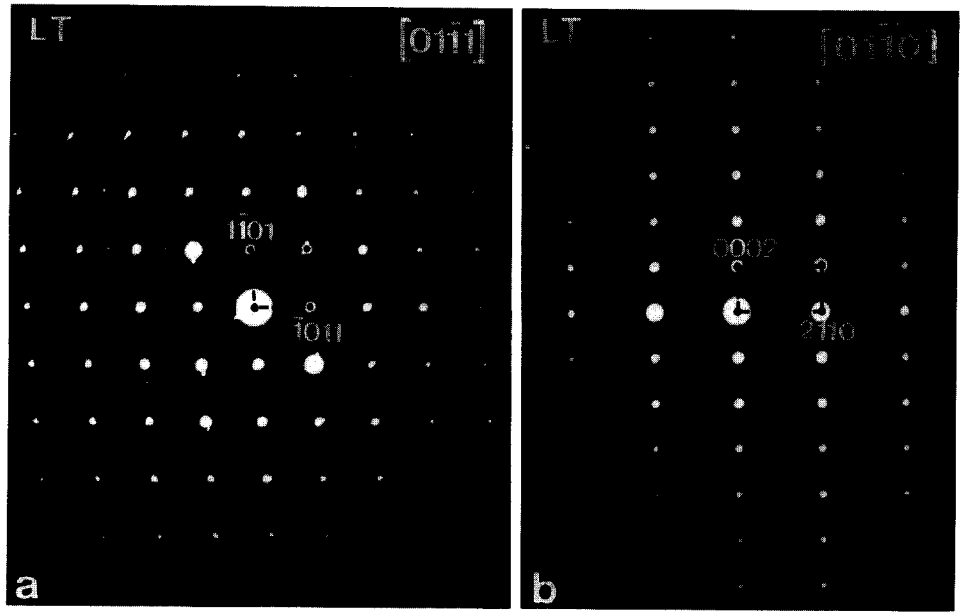

Fig. 14. Low-temperature diffraction patterns of HCP-grown C_{70}; the indices refer to the hexagonal parent lattice. (a) The [01$\bar{1}$1] section. (b) The [01$\bar{1}$0] section.

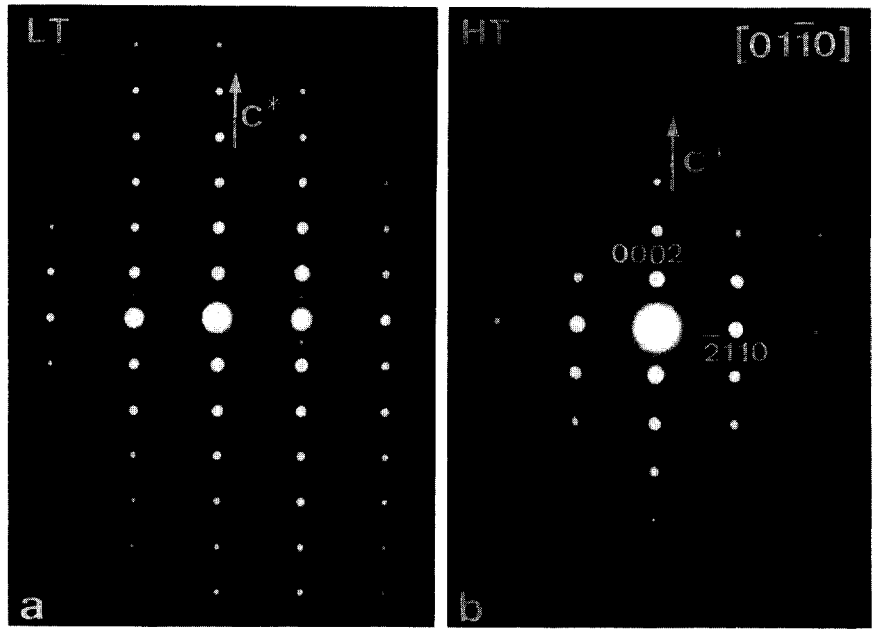

Fig. 15. [0$\bar{1}$10] diffraction pattern of HCP-grown C_{70} crystals taken from the same area: (a) at low temperatures, below 270 K; (b) above the transition of 337 K.

a Shockley partial and may possibly have been introduced by deformation along the close-packed planes during sample preparation. Rather exceptionally also a single layer fault of the type ABABCBCBC... was observed; such a fault cannot be formed by the motion of a Shockley partial.

The dot arrays also allow one to measure the c/a value in direct space; from fig. 13b we find at room temperature for the HCP phase $c/a = 1.64 \pm 0.03$, which is slightly different from the ideal value. The corresponding ratio can also be deduced from the FCC bands; within the rather large measuring error, due to the finite width of these bands, it is found not to be significantly different. The FCC bands are sometimes twinned as in fig. 13a and faulted by intrinsic faults.

Around room temperature the c/a ratio of the hexagonal phase seems to be very sensitive to the sample temperature; this is suggested by the difference which is sometimes observed between the c/a ratio deduced from the diffraction pattern ($c/a = 1.82$), taken with a relatively low-intensity beam and the c/a ratio derived from the high-resolution image ($c/a = 1.64$), for which an intense electron beam is used. The temperature difference due to the beam heating is apparently responsible for the rather drastic change in c/a value. Recent Raman and X-ray measurements [21] attribute this drastic c/a change to the 337 K transition reported in ref. [9].

4.2. Low-temperature structure

When cooling HCP-grown crystals we observe another phase transition around 270 K. The superstructure associated with the low-temperature phase causes weak supplementary spots to appear in the different sections and causes furthermore the extinctions of the $000l$ reflections (l = odd), which normally apply to the hexagonally close-packed structure, to be violated (fig. 14b). The spots with l = odd in the sequence $000l$ appear in the $[01\bar{1}0]$ section, where normally all spots with l = odd are absent (fig. 15b). Unlike in the $[2\bar{1}\bar{1}0]$ section such spots cannot be caused by double diffraction. The c_0 parameter as deduced from fig. 14b is found to be $c_0 = 1.85$ nm; the corresponding c/a ratio is then approximately 1.83. When the sample is heated again slightly above room temperature, the superstructure reflections disappear and the c/a ratio becomes $c/a = 1.64$, i.e. only slightly larger than the ideal value for HCP (figs. 15a and 15b).

In the section $(0001)^*_{HCP}$ no superstructure spots are detected but in the slightly inclined $[01\bar{1}1]$ section of fig. 14a the $[\bar{1}011]^*$ row of reflections exhibits superstructure spots halfway

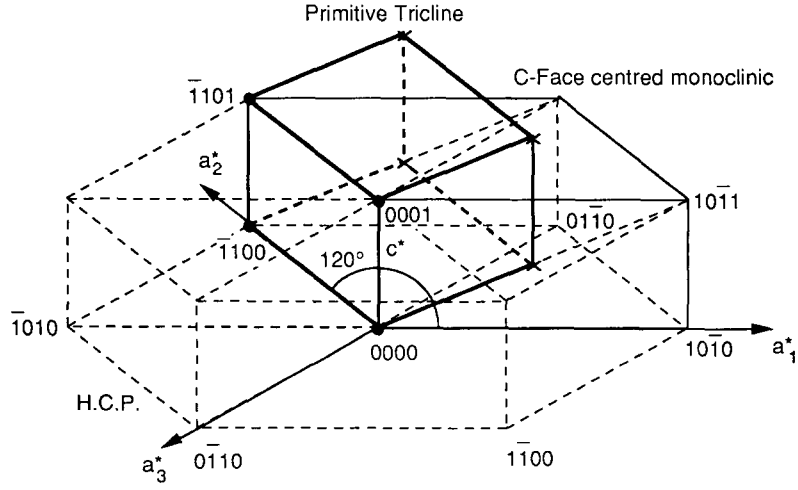

Fig. 16. Schematic representation of the reciprocal lattice as deduced from different sections of reciprocal space such as in fig. 14.

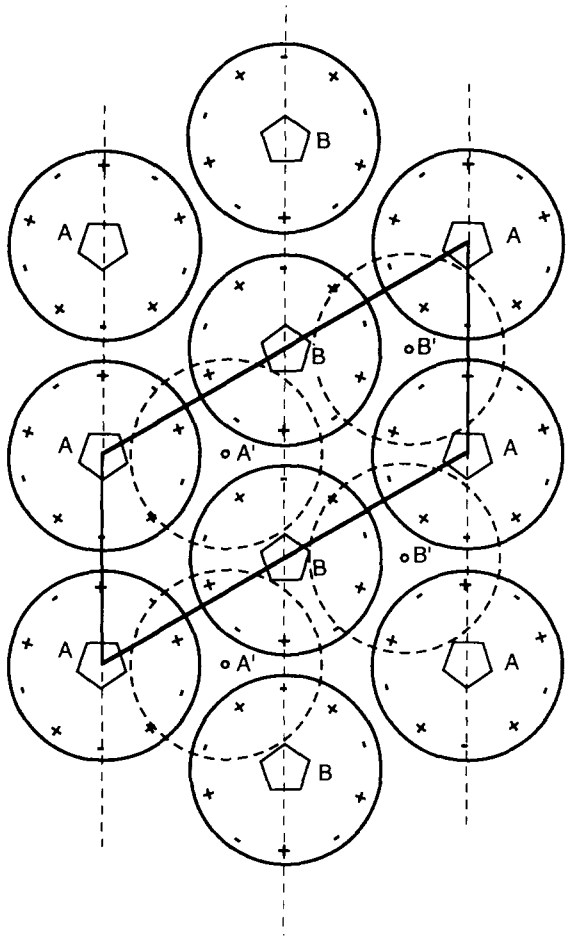

Fig. 17. Model for the low-temperature monoclinic distorted structure of C_{70}, imaged along the pseudo-hexagonal c-axis. A and B refer to C_{70} molecules rotated 180° with respect to each other; + and − signs indicate electron-rich and electron-poor areas along the equator of the molecule. (A, B) and (A', B') refer to the two different sublattices in the C-centered monoclinic unit cell which is outlined here.

between the basic HCP spots. No supplementary spots appear in the symmetry-related row $[1\bar{1}01]^*$, however. From several such sections of reciprocal space the reciprocal lattice was constructed; the reciprocal unit cell has become C-face-centered monoclinic with a β angle close to 120° (fig. 16).

The unit cell of the corresponding direct space lattice, which is also face-centered monoclinic, is shown in fig. 17. It is quite clearly a supercell of the HCP unit cell, perhaps with a β angle slightly different from 120°, the deviation being too small to be observable in electron diffraction. If we call $\boldsymbol{a}_{1,\mathrm{H}}$, $\boldsymbol{a}_{2,\mathrm{H}}$ and $\boldsymbol{c}_{\mathrm{H}}$ the base vectors of the HCP lattice the base vectors of the monoclinic lattice are given by

$$\boldsymbol{a}_{\mathrm{M}} = \boldsymbol{a}_{2,\mathrm{H}},$$
$$\boldsymbol{b}_{\mathrm{M}} = 2\boldsymbol{c}_{\mathrm{H}},$$
$$\boldsymbol{c}_{\mathrm{M}} = 2\boldsymbol{a}_{1,\mathrm{H}},$$

or

$$\begin{pmatrix} \boldsymbol{a}_{\mathrm{M}} \\ \boldsymbol{b}_{\mathrm{M}} \\ \boldsymbol{c}_{\mathrm{M}} \end{pmatrix} = \begin{pmatrix} 0 & 1 & 0 \\ 0 & 0 & 2 \\ 2 & 0 & 0 \end{pmatrix} \begin{pmatrix} \boldsymbol{a}_{1,\mathrm{H}} \\ \boldsymbol{a}_{2,\mathrm{H}} \\ \boldsymbol{c}_{\mathrm{H}} \end{pmatrix}.$$

We have hereby ignored a possible small deformation of the hexagonal lattice. The C-face is, moreover, centered, i.e. there is a lattice point at $\boldsymbol{a}_{2,\mathrm{H}} + \boldsymbol{c}_{\mathrm{H}}$. The primitive unit cell is triclinic, with base vectors defined for instance as:

$$\boldsymbol{a}_{\mathrm{T}} = \boldsymbol{a}_{2,\mathrm{H}},$$
$$\boldsymbol{b}_{\mathrm{T}} = \boldsymbol{a}_{1,\mathrm{H}} + \boldsymbol{c}_{\mathrm{H}},$$
$$\boldsymbol{c}_{\mathrm{T}} = 2\boldsymbol{c}_{\mathrm{H}},$$

or

$$\begin{pmatrix} \boldsymbol{a}_{\mathrm{T}} \\ \boldsymbol{b}_{\mathrm{T}} \\ \boldsymbol{c}_{\mathrm{T}} \end{pmatrix} = \begin{pmatrix} 0 & 1 & 0 \\ 1 & 0 & 1 \\ 0 & 0 & 2 \end{pmatrix} \begin{pmatrix} \boldsymbol{a}_{1,\mathrm{H}} \\ \boldsymbol{a}_{2,\mathrm{H}} \\ \boldsymbol{c}_{\mathrm{H}} \end{pmatrix}.$$

The diffraction conditions of this phase are compatible with the space groups Cm and C2.

Since the basic lattice of which all node points are occupied by molecules has not changed appreciably it is very likely that the structure built on this monoclinic lattice must be an orientationally ordered superstructure of the HCP stacking of close-packed layers of C_{70} molecules, with their length axis parallel to the c-axis of the HCP lattice. The latter feature is strongly suggested by the corresponding c/a ratio (1.82), which is very nearly equal to the value of the ideal HCP stacking of spheres ($c/a = 1.63$) multiplied by the aspect ratio of the C_{70} molecule (1.12).

Four-circle single-crystal X-ray diffraction experiments as well as electron diffraction measurements made on a different hexagonal crystal have given evidence for the occurrence of a second,

more abundant low-temperature phase. This phase gives rise to superstructure spots midway between the basic spots along all $[10\bar{1}0]_H$ directions, related by hexagonal symmetry, but produced no evidence for a superperiod along the [0001]* direction. In view of the electron diffraction results it is believed that the apparent hexagonal structure has in fact a primitive monoclinic lattice with a β angle of 120°, the a-parameter being doubled along one $[10\bar{1}0]_H$ direction only. The base vectors of the monoclinic lattice are now related to those of the hexagonal parent structure by the relations

$$a_m = a_{2,h}; \quad b_m = c_h; \quad c_m = 2a_{1,h}.$$

The diffraction conditions are compatible with the space group and $P2_1/m$. The two phases have closely related structures, both superstructures of the HCP structure. Details on the molecular arrangement in both phases are given in refs. [23,24].

4.3. High-temperature structure

At higher temperatures above room temperature, the structure of C_{70} is based on an AB-CABC stacking [9]; however, we find that the structure is only pseudo-cubic, the unit cell being elongated along the [111] direction which at low temperature corresponded to the $[0001]_{hex}$ direction (see fig. 12). When the temperature is raised inside the electron microscope the diffraction patterns gradually acquire cubic symmetry; i.e. the rhombohedral distortion becomes smaller and smaller, as deduced from electron diffraction evidence.

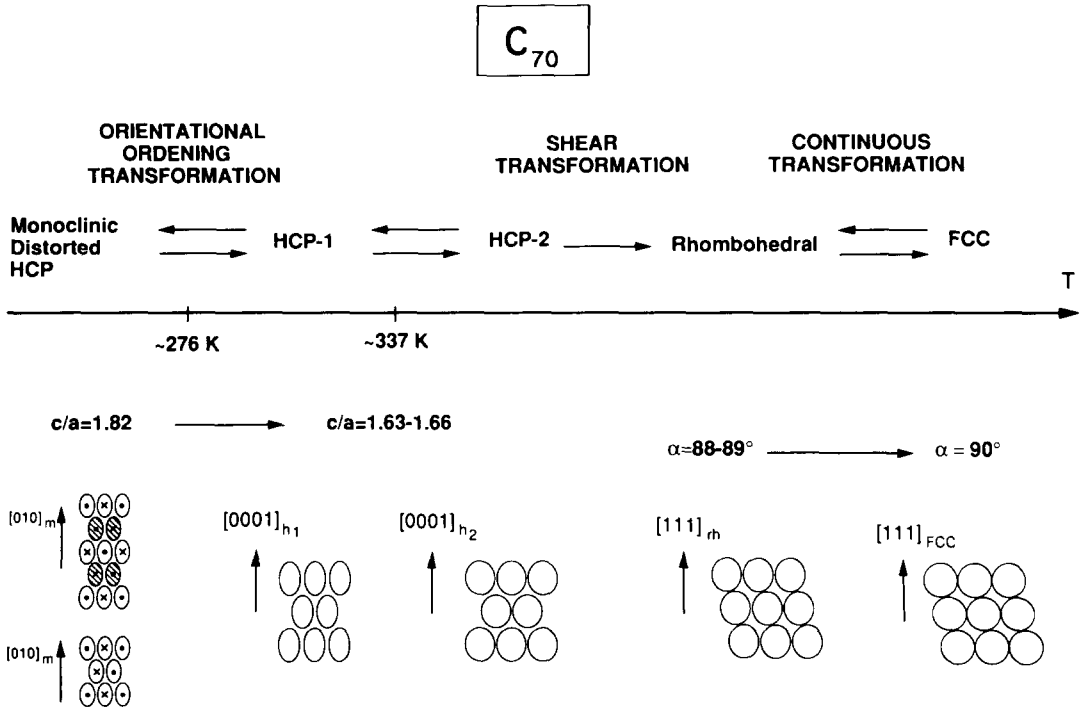

Fig. 18. Schematic representation of the different phase transformations occurring in C_{70} crystals.

4.4. Model for the phase transformations

All observations seem to be compatible with a model in which the molecular axes are highly preferentially oriented along the c-direction of a hexagonally stacked crystal at the lowest temperature, leading at low temperature to a c/a ratio of 1.82. As the temperature is raised first the molecular rotations with their long axis along the c-axis are excited. As the temperature is further raised the time-averaged orientation of the molecular axis still coincides with the c-direction of the hexagonal crystal, but it may instantaneously adopt other orientations as well, resulting in a – sudden – decrease of the c/a ratio. This would be the transition at 337 K reported in ref. [9].

At higher temperatures when the instantaneous rotation axis becomes almost isotropically distributed the crystal undergoes a shear transformation into a slightly rhombohedral crystal in which the time-averaged molecular axis is still somewhat preferentially oriented along the [111] direction which results from the [0001] direction after transformation. At still higher temperatures the crystal will gradually become FCC, the rotations then being completely random. A schematic representation of the different phases occurring in C_{70} as a function of temperature is given in fig. 18.

A microscopic model for the structure of the low-temperature monoclinic superstructure can be deduced from the different reciprocal sections and assuming that the stacking principle is the same as that found for the C_{60} molecules in the simple cubic structure. According to this principle the regions of large electron density along covalent bonds, i.e. along 6-5 and 6-6 edges of the C-cage, tend to face the regions of low electron density of the adjacent molecules, i.e. along the side faces of the cage. Application of this principle to the C_{70} molecules in the close-packed layers leads to the following model. The molecular cages come closest to one another along their equators. Along the equator five electron-rich regions along the 6-6 edges alternate with five electron-poor regions, along the centres of the hexagonal faces. The stacking corresponding to the smallest electrostatic energy, i.e. the most uniform distribution of the electron density, is one in which electron-poor regions (indicated by a – sign in fig. 17) face electron-rich regions (indicated by a + sign in fig. 17) to the largest extent possible.

Applying this principle to one close-packed row of molecules, one finds that these must be arranged as shown in fig. 17, i.e. all molecules are in parallel orientations. However, such an energetically favourable arrangement can only be achieved along one close-packed direction. In order to achieve the optimum 2D configuration, the molecules in two adjacent parallel rows must differ 180° (or 36°) in orientation. It is clear from fig. 17 that then electron-rich and electron-poor regions face each other not only within one row but also to a good approximation betweeen adjacent rows. The resulting structure leads to doubling of the unit cell size in the c-direction of the HCP basic lattice and is consistent with the centering of the C-face of the monoclinic lattice. It also leads to doubling of the repeat distance along two out of three of the a-directions of the HCP lattice, breaking the hexagonal symmetry, but due to the extinctions as a result of C-centering of the unit cell this does not create superstructure spots in the (0001)* section. The molecules have to be stacked in the described way in all "a" layers of the abababa... HCP stacking. Also all "b" layers have to be stacked in a similar manner. In fig. 17 we have indicated the two molecular orientations in the a-layer by A and B, and in the b-layer by A′ and B′. From fig. 17 we can conclude that the structure contains four interpenetrating C-centered monoclinic sublattices, each sublattice being occupied by molecules of a given orientation either A, B, A′ or B′. The stacking considerations used here do not allow us to conclude unambiguously whether A = A′ and B = B′ or alternatively A = B′ and B = A′. The four sublattices of oriented molecules are related by the lost symmetry translations of the HCP structure. Details of this model have been presented in ref. [22]; the primitive monoclinic superstructure has been described in detail in refs. [23,24].

It is evident that the described structure can

be formed in six orientation variants within a given HCP stacking. Each orientation variant can, moreover, be formed in four different translation variants corresponding to the fourfold unit cell as compared to the HCP unit cell. Single variants of the HCP phase are therefore likely to be fragmented in up to as many as 24 structural variants of the ordered phase. This will hamper, to some extent, single-crystal studies by X-ray diffraction.

4.5. Discussion

The intimate mixture at room temperature (after liquid-nitrogen crushing) of HCP and FCC bands limited by close-packed planes is characteristic for the microstructure resulting from an incomplete shear transformation HCP ⇒ FCC, performed by the nucleation and motion of Shockley partial dislocations. It is most probable that the transformation occurred from the HCP phase towards the FCC phase since the transformation defects are located on a single family of close-packed planes. If the parent phase were FCC and the product phase HCP, the transformation would have taken place with equal probability on all {111} families of planes and the resulting microtexture would have consisted of four hexagonal variants. The observation at room temperature of a mixture of FCC and HCP is presumably due to the fact that the shear transformation, which is very sluggish, apparently takes place over a wide temperature range, centered somewhat above room temperature.

Since the last temperature cycle before observation consisted of heating from liquid-nitrogen temperature, where the sample was crushed, to the observation temperature, it is likely that a shear transformation in the sense HCP ⇒ FCC has taken place somewhere below the observation temperature, which is somewhat above room temperature. This, in turn, implies that below the transition temperature the stable phase is HCP and above this temperature FCC. The HCP ⇒ FCC transition presumably occurs at the temperature where the molecules start behaving approximately as spheres.

The succession of phase transitions occurring in the HCP-based phase, starting from the low-temperature side, can be visualised as follows.

The first type of disorder created on heating consists of the excitation of rotational modes about the c-direction, i.e. about the long axis of the molecule. Since for such rotations there is no steric hindrance, such rotations will presumably be the easiest ones to be excited at the lower temperatures. In this state the crystal is hexagonally close-packed with a c/a ratio of 1.82; the long axis of the molecules, which have now cylindrical symmetry, are still parallel. The onset of such rotations corresponds with a transition monoclinic-to-hexagonal ($c/a = 1.82$).

With increasing temperature, rotational modes about axes other than the length axis are excited, which leads to a decrease of the c/a ratio down to 1.66–1.64; the molecules become more or less spherical. The c/a ratio is somewhat variable and with increasing temperature it decreases until $c/a = 1.63$. The transition from HCP-1 ($c/a = 1.82$) into HCP-2 ($c/a = 1.66$) apparently occurs over a relatively small temperature interval and corresponds with a cooperative phase transformation.

The shear transformation from HCP-2 with abab... stacking into a rhombohedral one with abcabc... stacking and c/a ratio slightly above the ideal value for close-packing of spheres must presumably be associated with a somewhat higher temperature and is preceded by an increasing excitation of rotations about axes other than the still slightly preferentially oriented long axis. The rotations become gradually more isotropic, but the molecules still spend more than the statistically average fraction of their time with their long axis parallel to the c_H axis. This causes the abcabc... stacking to be slightly rhombohedral, the threefold axis being parallel to the original c-axis of the HCP phase. This relationship is consistent with the shear character of the transformation since steric hindrance has to be overcome.

With further increasing temperature the molecules start rotating freely and isotropically and the structure becomes FCC, the molecules being effectively spherical; the lattice parameter of the FCC phase ($a = 1.496$ nm) is then some-

what larger than that of the FCC phase of C_{60} (a = 1.417 nm). The series of phase transformations as deduced from these electron diffraction experiments are represented schematically in fig. 18.

Acknowledgements

The authors are particularly grateful to M.O. Ruault for helping with the liquid-He experiments at the University Paris-Sud (Orsay). This work has been made possible with the financial help of the National Fund for Scientific Research (Belgium) and of the Services for Science Policy (IUAP 11) of the National Government (Belgium). Part of this work has been possible with the financial support of the Dutch Organisation for Fundamental Research of Matter (FOM).

References

[1] R.M. Fleming, T. Siegrist, P.M. Marsh, B. Hessen, A.R. Kortan, D.W. Murphy, R.C. Haddon, R. Tycko, G. Dabbagh, A.M. Mujsce, M.L. Kaplan and S.M. Zahurac, Mater. Res. Soc. Symp. Proc. 206 (1991) 691.
[2] R.E. Smalley, "The almost (but never quite) complete Buckminsterfullerene bibliography", available on request ("Buckybib", Department of Chemistry, Rice University, P.O. Box 1892, Houston, TX 77251, USA).
[3] D. Huffman, Phys. Today (November 1991) 22.
[4] G. Van Tendeloo, M. Op de Beeck, S. Amelinckx, J. Bohr and W. Krätschmer, Europhys. Lett. 15 (1991) 295.
[5] A. Dworkin et al., C.R. Acad. Sci. Paris 312, Sér. II (1991) 665.
[6] P.A. Heiney, J.E. Fisher, A.R. Mc Ghie, W.J. Romanow, A.M. Denenstein, J.P. Mc Cauley, Jr., A.B. Smith III and D.E. Cox, Phys. Rev. Lett. 66 (1991) 2911.
[7] D.A. Neumann et al., Phys. Rev. Lett. 67 (1991) 3808.
[8] W.I.F. David, R.M. Ibberson, J.C. Matthewman, K. Prassides, T.J.S. Dennis, J.P. Hare, H.W. Kroto, R. Taylor and D.R.M. Walton, Nature 353 (1991) 147.
[9] G.B.M. Vaughan, P.A. Heiney, J.E. Fischer, D.E. Luzzi, D.A. Ricketts-Foot, A.R. McGhie, Y.W. Hui, A.L. Smith, D.E. Cox, W.J. Romanow, B.H. Allen, N. Coustel, J.P. McCauley, Jr. and A.B. Smith III, Science 254 (1991) 1350.
[10] W. Krätschmer, L.D. Lamb, F. Fostiropoulos and D.R. Huffman, Nature 347 (1990) 354.
[11] H. Aije, M.M. Alvarez, S.J. Anz, R.K. Beck, F. Diederich, K. Fostiropoulos, D.R. Huffman, W. Krätschmer, Y. Rubin, K.E. Shriver, D. Sensharma and R.L. Whetten, J. Phys. Chem. 94 (1990) S630.
[12] M.A. Verheijen, H. Meekes, G. Meijer, E. Raas and P. Bennema, Chem. Phys. Lett. 191 (1992) 339.
[13] P.A. Heiney et al., Phys. Rev. B, submitted (Rapid Communication).
[14] S. Amelinckx, C. Van Heurck, D. Van Dyck and G. Van Tendeloo, Phys. Status Solidi (a) 131 (1992) 589.
[15] R. Sachidanandam and A.B. Harris, Phys. Rev. Lett. 67 (1991) 1467.
[16] S. Liu, Y.-J. Lu, M.M. Kappes and J.A. Ibers, Science 254 (1991) 408.
[17] J. De Boer et al., private communication.
[18] K. Michel, Chem. Phys. Lett. 193 (1992) 478.
[19] W.I.F. David, R.M. Ibberson, T.J.S. Dennis, J.P. Hare and K. Prassides, Europhys. Lett. 18 (1992) 219.
[20] S. Muto, G. Van Tendeloo and S. Amelinckx, Phil. Mag., submitted.
[21] M.A. Verheijen et al., J. Phys. Chem., in press.
[22] G. Van Tendeloo and S. Amelinckx, at the "Frontiers of Electron Microscopy in Materials Science", Oakland, April 24–27, 1992.
[23] G. Van Tendeloo, S. Amelinckx, J.L. de Boer, S. Van Smaalen, M.A. Verheijen, H. Meekes and G. Meijer, Europhys. Lett. 21 (1993) 329.
[24] M.A. Verheijen, H. Meekes, G. Meijer, J.L. de Boer, S. Van Smaalen, G. Van Tendeloo, S. Amelinckx, S. Muto and J. Van Landuyt, Chem. Phys. 166 (1992) 287.